Neutron capture and total cross sections of ^{144}Sm

R. L. Macklin, N. W. Hill, J. A. Harvey,* and G. L. Tweed†
Oak Ridge National Laboratory, Oak Ridge, Tennessee 37831
(Received 26 April 1993)

Neutron capture and transmission measurements have been made from 0.5 eV to 500 keV and have been analyzed to give parameters of resonances up to ~100 keV. The average resonance spacing for *s*-wave resonances was determined to be 670±60 eV and the *s*-wave strength function $(3.6\pm0.8)\times10^{-4}$. The average radiation width for *s*-wave resonances was 74±5 meV and that for *p*-wave resonances somewhat larger ~89 meV. The Maxwellian average capture cross section at a stellar temperature of 30 keV was 92±6 mb. The capture resonance integral of 1.7±0.1 b calculated from the resonance parameters and the thermal cross section is smaller than the recently measured value of 2.38±0.17 b.

PACS number(s): 28.20.−v, 27.60.+j

I. INTRODUCTION

In the nuclear shell model ^{144}Sm exhibits a closed shell of 82 neutrons. Neutron resonance parameters of the other four stable nuclides with 82 neutrons have been measured and their average level spacings and *s*-wave neutron strength functions have been determined. No neutron resonance data exist for ^{144}Sm and, hence, it was of interest to see how information on this nuclide compares to corresponding information of the other four $N=82$ stable nuclides.

The nuclide ^{144}Sm is only a minor product of nucleosynthesis in stars, in contrast to some other closed shell nuclei which lie in the main neutron capture sequence above iron in atomic mass. As the lightest and least abundant (3.1%) of the samarium isotopes, it is thought to have been formed from the heavier ones in a brief episode of intense (γ,n) reactions in a rare stellar environment.

The neutron resonance structure and the capture cross section of ^{144}Sm are also of interest for the production of ^{145}Pm by neutron irradiation of ^{144}Sm in a nuclear reactor, followed by electron capture decay of ^{145}Sm. Recent experimental studies have been confined to thermal and $1/E$ neutron spectra [1] and one measurement [2] of average capture cross section from 5- to 350-keV neutron energy. ^{144}Sm has been included in a recent Hauser-Feshbach calculation and evaluation of neutron capture cross sections [3]. The present study covers the energy range from 0.5 eV to 500 keV with sufficient energy resolution to yield cross-section data which can be parametrized to produce resonance parameters for a large number of individual resonances.

*Please direct all correspondence to J. A. Harvey, Oak Ridge National Laboratory, Building 6010, MS-6356, P.O. Box 2008, Oak Ridge, TN 37831-6356; telephone (615) 574-4489, FAX (615) 576-8746.

†Currently at Systematic Management Services, Inc., Oak Ridge, TN 37830.

II. EXPERIMENTAL PROCEDURE

A. Capture measurements

Measurements of prompt neutron capture in the sample were made as a function of neutron time of flight at the Oak Ridge Electron Accelerator (ORELA) 40-m station. Descriptions of the detectors and monitors used have been presented previously in a paper describing similar measurements on four tungsten isotopes [4]. Most of the systematic uncertainties associated with the apparatus and analysis also have been discussed and tabulated elsewhere [5,6].

The experimental procedure involved positioning the sample within the flight path and using a total energy detector for measuring the prompt gamma rays emitted following the capture of a neutron by the sample. The capture gamma rays were detected by a pair of nonhydrogenous liquid scintillators and the total gamma-ray energy was calculated by the pulse-height weighting method [7]. The detection efficiency was determined by the 4.9-eV saturated gold resonance method [8] using a thin ^{6}Li glass scintillator as a neutron flux monitor [9]. The neutron energy scale adopted was that of the 80-m neutron transmission measurements described below.

The samarium oxide, Sm_2O_3, powder sample for the capture measurement was compressed to a 25.4-mm-diameter disk 1.3 mm thick, weighing 2.284 g. It was initially bound together by 99 mg of admixed camphor, but this was pumped away in the evacuated flight path before the capture measurements were started. The areal density was thus 0.00156 atom of ^{144}Sm per barn. Isotopic and elemental analyses of the sample material are shown in Table I.

Four measurements of neutron capture yield were made, covering four different energy ranges: 1–2.5 eV, 2.5–13 eV, 11–9850 eV, and 2.6–500 keV. For the first two ranges, a cadmium filter was used to eliminate neutrons below 0.5 eV, and the ORELA accelerator was operated at 220 pulses per second for four hours in each energy range. For the two higher energy ranges, a 0.48-g/cm^2 ^{10}B filter was used and the accelerator operated at

TABLE I. Enriched $^{144}Sm_2O_3$ analyses.

Isotope or element	Composition (at. %)	Uncertainty (%)
^{144}Sm	96.47	0.05
^{147}Sm	1.08	0.01
^{148}Sm	0.56	0.01
^{149}Sm	0.54	0.01
^{150}Sm	0.24	0.01
^{152}Sm	0.65	0.01
^{154}Sm	0.46	0.01
Ce, Dy	not found	<0.1 wt. %
Other rare earths	not found	<0.002 to <0.05 wt. %
Mg	trace	<0.01 wt. %
Others	not found	<0.001 to <0.2 wt. %

800 pulses per second for 39 h for the 11- to 9851-eV energy range and for 84 h for the highest energy range.

B. Transmission measurements

Four transmission measurements were made by the time-of-flight technique using neutron pulses from the ORELA water-moderated tantalum target. Two ^{6}Li glass scintillation detectors and one NE-110 detector were used. For all measurements water-moderated neutrons were used.

For the lowest energy measurements down to 0.5 eV, a 1-mm-thick ^{6}Li glass detector at a 17.909-m flight path was used resulting in an energy resolution of 0.3%. The ^{6}Li scintillator was 10 cm in diameter, mounted in a 0.025-mm-thick, 15-cm-diameter Mylar reflecting cylinder between two RCA-8854 photomultiplier (PM) tubes. The accelerator was operated at a pulse repetition rate of 347 pps (20 ns wide pulses and 12 kW) and a 1.5-mm cadmium filter was used to prevent overlap.

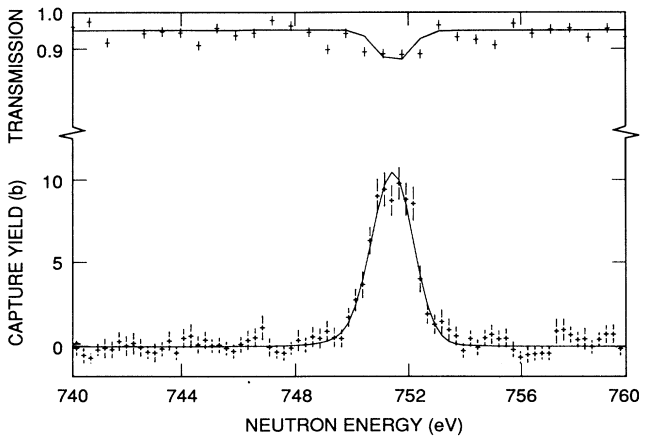

FIG. 1. The lowest energy resonance peak clearly identifiable as due to ^{144}Sm. The upper part of the figure shows the transmission for the thick sample, the statistical uncertainties and the computed fitting curve. The lower part shows the capture yield for the thin sample and the fitted curve. The resonance parameters found are included in Table II.

For higher energy resolution measurements an 80.394-m flight path was used resulting in an energy resolution <0.1%. For measurements up to $\sim$60 keV, a 12.5-mm-thick ^{6}Li glass scintillator, 11.1 cm in diameter mounted in a similar cylinder between two RCA-8854 photomultiplier tubes, was used. The accelerator was operated at

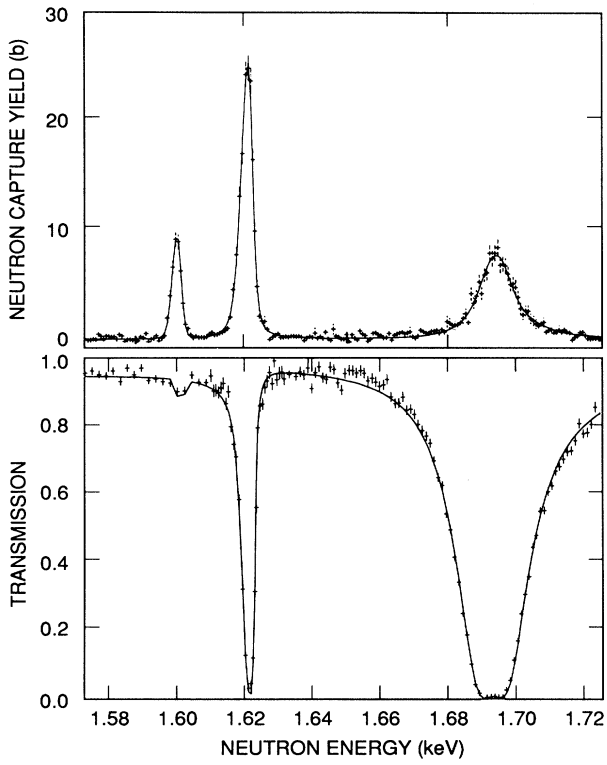

FIG. 2. Three typical resonance peaks in the reaction ^{144}Sm+n. The lower part of the figure shows the transmission for the thick sample, the statistical uncertainties and the computed fitting curve. The upper part shows the capture yield points for the thin sample and the fitted curve. The resonance parameters found are included in Table II. The shapes for the lowest energy resonance are dominated by the instrumental resolution and Doppler broadening whereas the other two resonances show increased breadth due to their larger total widths.

TABLE II. $^{144}Sm+n$ resonances below 12 keV.

E_0 (eV)[a]	$g\Gamma_n$ (eV)	$g\Gamma_\gamma\Gamma_n/\Gamma$ (meV)[b]	Γ_γ (meV)	l
751.6	0.0041(4)[c]	3.6(1)		1
1023.0	0.0174(8)	15.4(1)		1
1186.9	0.0833(16)	29.0(2)		1
1262.5	<0.010	3.7(3)		1
1602.5	0.0115(24)	11.8(4)		1
1621.9	0.824(9)	61.0(14)	65.9(17)	0
1693.0	6.693(22)	62.2(17)	62.8(17)	0
1895.1	0.016(2)	11.3(5)		1
1982.3	0.106(3)	40.1(9)	64.6(14)	1
2071.1		7.2(5)		1
2279.1	0.048(4)	36.5(9)		1
2584.6	6.51(3)	58.8(21)	59.3(21)	0
2824.7	0.030(5)	27.8(7)		1
3043.1	11.36(5)	103.4(27)	104.3(27)	0
3154.2		13.2(6)		1
3411.8		19.8(11)		1
3777.0		7.5(7)		1
3875.7		4.7(13)		1
3881.3	<0.050	7.6(9)		1
4042.0	14.37(7)	72.2(30)	72.6(30)	0
4295.2	0.046(10)	30.9(11)		1
4480.7		6.8(15)		1
4487.3	2.68(4)	61.7(21)	63.6(22)	0
4534.1		13.2(10)		1
4639.1	78.45(20)	121.(14)	121.(14)	0
4744.3	0.049(17)	25.7(13)		1
4902.6	0.160(24)	49.6(17)		1
5193.6	0.090(24)	46.8(19)		1
5567.4	9.25(8)	49.(3)	49.(3)	0
5820.0	0.222(24)	77.1(30)	118.(6)	1
5984.7		33.0(19)		1
6062.1		9.0(14)		1
6160.7	0.70(3)	53.0(22)	57.4(25)	0
6394.4		19.6(16)		1
6549.6	0.160(28)	65.1(24)		1
6904.8	0.31(3)	86.(4)	119.(6)	1
7145.8		24.7(18)		1
7313.5		39.2(26)		1
7326.3		34.3(27)		1
7483.2	0.40(4)	60.1(28)	71.(3)	0
7722.4		25.0(23)		1
7759.4		8.4(18)		1
7848.5		7.(2)		1
8009.7	<0.2	39.(4)	54.(5)	1
8085.9	29.92(23)	79.(9)	79.(9)	0
8266.3		6.9(22)		1
8304.6		6.7(23)		1
8441.8		5.3(23)		1
8495.6[d]	0.25(5)	99.(5)		1
8590.0		52.(4)		1
8729.7		8.2(24)		1
8891.7	50.4(3)	89.(18)	89.(18)	0
9036.0		5.7(21)		1
9598.0		38.(3)		1
9812.1		62.(4)		1
9887.2	0.31(8)	77.(4)		(0)
10 153	<0.2	72.(4)		1
10 208		13.(3)		1
10 309	0.35(10)	59.(4)		1

TABLE II. (*Continued*).

E_0 (eV)[a]	$g\Gamma_n$ (eV)	$g\Gamma_\gamma\Gamma_n/\Gamma$ (meV)[b]	Γ_γ (meV)	l
10 386	32.1(3)	83.(11)	83.(11)	0
10 512		52.(4)		1
10 565		19.(3)		1
10 646		13.(4)		1
10 696		11.(4)		1
10 792		42.(4)		1
10 905	0.94(29)	70.(6)	76.(6)	(0)
11 280[d]	1.7(6)	125.(7)		0
11 333		11.(4)		1
11 413		16.(4)		1
11 503	136.8(8)	64.(26)	64.(26)	0
11 591		37.(6)		1
11 735		35.(4)		1
11 808	0.13(8)	73.(5)		1
11 917	3.07(16)	62.(8)	62.(8)	0

[a]Uncertainty in the laboratory energy scale is estimated as $\pm 0.01\%$.
[b]The capture kernels are shown with their statistical standard deviations of fitting. Calibration and other systematic uncertainties are less than 4%.
[c]Uncertainties in the last decimal(s) are shown in parentheses and are the Baysean standard deviations from the SAMMY program covariance matrix. Systematic uncertainties are $\lesssim 2\%$.
[d]Appears to be a doublet in the capture data.

1000 pps with 25-ns wide pulses and a 0.5-gm/cm^2 ^{10}B filter was used to reduce overlap neutrons to $<1\%$.

For high resolution data above ~ 10 keV, a detector consisting of a 5×5-cm^2 NE-110 scintillator, 2.5-cm thick, epoxy coupled to two 12.5-cm diameter RCA-8854 photomultipliers was used. The accelerator was operated at 800 pps with 8-ns wide pulses and a 0.5-gm/cm^2 ^{10}B filter was used to reduce backgrounds due to low energy neutrons. Each PM was biased below the single photoelectron level and a coincidence was required between the two outputs of the two PMs to eliminate counts due to PM noise, similar to the technique discussed in Ref. [10].

A 0.6-cm-thick Pb filter was used for all four measurements to reduce the background associated with the gamma flash from the target. The photomultiplier bases were gated to eliminate the gamma flash from the target.

Two sample thicknesses of $^{144}Sm_2O_3$ were used in these transmission measurements. The sample used for the capture measurements (0.001 56 ^{144}Sm atom per barn) was used directly for the first transmission measurement at 80.394 m with the 12.5-mm-thick ^{6}Li glass scintillator. The sample was then reprocessed to powder and loaded in a tubular container for the other three transmission measurements with a sample thickness of 0.006 91 Sm atom/barn. By using a compensator of 77.7 mg of natural Sm_2O_3 for the open beam measurements, the effective contributions of the other Sm isotopes were reduced to $\ll 1\%$, so that an effective ^{144}Sm enrichment of 99.61% was achieved.

With this thicker sample, all the ^{144}Sm resonances seen in the capture measurements up to 2 keV could be discerned as shown in Table II. Examples are shown in Figs. 1 and 2. Additional resonances found only in the transmission data are listed separately in Table III. The transmission measurements made on the thicker sample using a NE-110 scintillation detector provided useful data in the energy range from 13 keV to 97 keV and those with the ^{6}Li scintillators provided useful data up to ~ 60 keV.

III. DATA PROCESSING AND RESULTS

A. Capture measurements

The neutron time-of-flight data were first corrected for electronic deadtime and rebinned into equal energy channels for analysis. The average capture cross-section data were additionally corrected for measured backgrounds as discussed in Ref. 11. Breit-Wigner parameters were fitted to the capture yield peaks up to 12 keV using the least squares program LSFIT [12] which included corrections for Doppler broadening and capture after single scattering. The experimental resolution function included in the code featured a convolution of Gaussian and exponential shapes. Examples of the fitted resonance peaks are shown in Figs. 1 and 2. Where resonance widths were determined for a resonance in addition to its capture area, the radiation width and capture kernel $g\Gamma_\gamma\Gamma_n/\Gamma$ were corrected for the scattered neutron sensitivity of the detectors. The correction factor was taken as one thousandth of the neutron width at 2219 eV and proportional to $E_n^{-1/2}$ as discussed in Refs. [11,13]. The resonance parameters found are included in Table II. Additional broad resonances from 13 keV to 97 keV derived from the neutron transmission measurements described below are shown in Table III. All the small resonance peaks seen at neutron energies from 1 eV to 750 eV correspond to known resonances of the samarium isotopes other than ^{144}Sm present in the sample (see Table I).

By combining the capture kernels with the neutron

widths from the transmission measurements (see below), radiation widths for a number of resonances were derived and are included in Table II. Sixteen radiation widths were obtained for s-wave resonances with an average value of 74±5 meV, where the uncertainty is the standard deviation of the mean. The sample standard deviation, 18.5 meV, together with the mean, correspond to a chi square distribution with 32 degrees of freedom. The four radiation widths assumed to be for p-wave resonances from discussion in the following section have an average value slightly larger ~89 MeV.

Average capture data are presented in three ways; broad energy band histograms above 6 keV (Table IV) and Fig. 3, Maxwellian averages as a function of stellar temperatures (Fig. 4), and the capture resonance integral. The contribution to the capture resonance integral from the measured resonances below 12 keV and the average capture cross section above 12 keV is 1.13±0.05 b. Attributing most of the (1.64±0.10) b thermal capture cross section [1] to $1/v$ dependent direct capture leads to a total resonance integral of 1.7±0.1 b.

The Maxwellian average capture at the conventional stellar nucleosynthesis temperature of 30 keV was found to be (92±6) mb, where most of the uncertainty is due to background corrections.

B. Transmission measurements

The transmission data were first corrected for the deadtime (1104 ns) of the time digitizer (<4% for all

TABLE III. Additional ^{144}Sm+n resonances from 13 keV to 97 keV.

E_0 (eV)	$g\Gamma_n$ (eV)	l	E_0 (eV)	$g\Gamma_n$ (eV)	l
13 017	0.67(12)	1	55 437	13.(4)	0
13 574	18.8(4)	0	56 074	31.(6)	0
14 055	20.9(4)	0	56 556	34.(7)	0
14 292	0.38(14)	1	57 562	24.(6)	0
14 818	150.1(11)	0	58 938	9.(4)	0
15 336	18.0(4)	0	60 692	18.(5)	0
16 704	37.4(7)	0	60 892	37.(7)	0
17 059	14.0(5)	0	61 762	61.(9)	0
18 065	22.6(6)	0	62 634	62.(11)	0
18 763	1.6(5)	0	62 858	158.(15)	0
18 881	4.6(4)	0	63 955	177.(18)	0
19 507	124.5(15)	0	64 146	90.(14)	0
19 901	6.0(4)	0	64 942	120.(14)	0
20 803	2.1(4)	0	65 563	30.(7)	0
21 597	1.5(4)	(0)	65 966	19.(6)	0
22 058	2.6(5)	0	66 403	114.(14)	0
22 647	25.3(9)	0	67 579	20.(6)	0
23 003	31.8(10)	0	69 528	155.(16)	0
23 550	22.2(9)	0	71 130	112.(16)	0
24 494	107.1(19)	0	75 217	129.(15)	0
25 327	13.1(8)	0	76 426	136.(17)	0
28 415	1.9(6)	1	77 493	151.(19)	0
29 068	30.2(14)	0	79 372	29.(8)	0
29 209	1.1(5)	1	80 114	41.(10)	0
29 716	107.6(25)	0	80 609	206.(22)	0
31 280	53.0(20)	0	84 257	13.(6)	0
34 378	19.5(17)	0	85 173	85.(15)	0
34 914	20.2(18)	0	85 840	29.(9)	0
38 410	13.0(16)	0	86 268	27.(9)	0
39 117	48.3(26)	0	87 882	82.(15)	0
42 025	20.6(22)	0	89 860	102.(18)	0
42 967	54.(3)	0	90 165	55.(15)	0
44 505	15.0(20)	1	90 317	80.(21)	0
47 018	125.(5)	0	90 406	14.(9)	0
48 971	148.(6)	0	90 897	169.(23)	0
49 938	132.(6)	0	93 177	59.(13)	0
51 007	108.(5)	0	93 458	19.(8)	0
51 957	8.0(23)	0	94 408	39.(11)	0
52 690	22.(5)	0	95 498	23.(9)	0
53 626	36.(7)	0	95 835	64.(15)	0
53 918	7.(3)	0	96 709	82.(17)	0
54 121	20.(5)	0			

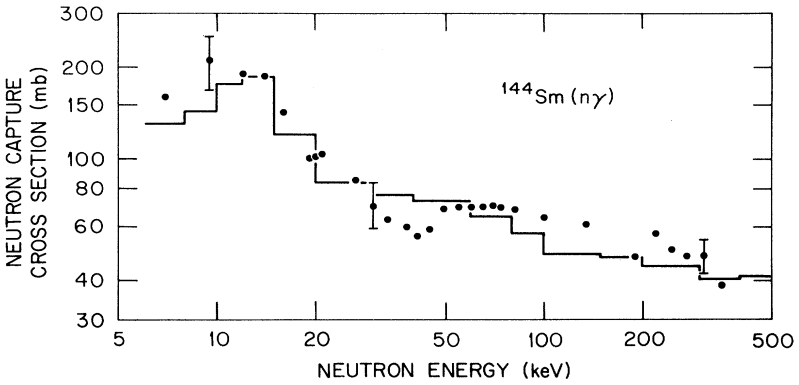

FIG. 3. Average neutron capture by ^{144}Sm. The solid circles and total uncertainties represent the data of Kononov *et al.* [2]; the histogram, the present data. Below 12 keV the histogram is derived from the individual resonance capture parameters shown in Table II. The standardization uncertainty of the present capture data (at the 68% probability level) is estimated to be ±4%.

measurements) and then corrected for several backgrounds (as discussed in Ref. [11]) which total $\lesssim 3\%$ over most of the energy regions which were analyzed. For the ^{6}Li glass scintillation detectors, these backgrounds consisted of a constant beam-independent background, a 17.6-μs gamma-ray background from the capture of the neutrons by the water moderator, overlap neutrons from the previous burst, and a time-dependent background arising from neutrons scattered from the ^{6}Li glass scintillator and scattered back to the scintillator. This latter effect produced a 0.3% tail on the resolution function. For the ^{6}Li glass scintillator detector measurements, the energy resolution was determined mainly by the moderation time in the target moderator which corresponds to a distance of <18 mm (FWHM) below 10 keV. For the NE-110 detector, in addition to the first three backgrounds listed above, there was a background due to resonance neutrons moderated in the scintillator and then escaping to be captured in the boron in the pyrex faces of the PMs producing a 478-keV gamma from the ^{10}B$(n,\alpha\gamma)$ reaction which can then be detected by the scintillator. To aid in the determination of the backgrounds and to optimize the signal-to-background ratio for this NE-110 detector, four separate pulse height spectra were recorded. The contribution from all backgrounds for this detector was $<1\%$ from 26 to 1800 keV and only 0.1% at 340 keV.

Parameters for the resonances were determined from the code SAMMY [14]. Resonances showing interference shapes in the transmission data were assigned as *s*-wave resonances. Three additional small resonances (at 9887, 10 905, and 21 597 eV) were also assumed *s* wave to improve the agreement with the Wigner and Δ_3 distribution laws [15,16]. The remaining resonances were assigned *p* wave (see Tables II and III). A plot of the 50 resonances identified as *s* wave, Fig. 5, drops significantly below a linear dependence at energies above 26 keV due to missed resonances at higher energies. The slope of the line from 1 keV to 26 keV corresponds to an average *s*-wave resonance spacing of (670±60) eV where the uncertainty is estimated from the limited number, 37, of resonances below 26 keV. A similar plot, Fig. 6, of the cumulative reduced neutron widths shows a roughly linear range up to the same energy, 26 keV, with a slope corresponding to an *s*-

TABLE IV. ^{144}Sm average neutron capture.

Energy range (keV)	Cross section (mb)[a]	Temperature kT (keV)	Maxwellian $\langle\sigma\rangle$ (mb)[a]
6–8	130[b]	5	217
8–10	143[b]	6	199
10–12	176[b]	8	173
12–15	185	10	155
15–20	120	15	126
20–30	84	20	110
30–40	77	25	100
40–60	73	30	92
60–80	65	35	86
80–100	57	40	82
100–150	49.1	50	75
150–200	48.2	60	70
200–300	45.0	70	67
300–400	40.9	85	63
400–500	41.7	100	60

[a]Systematic uncertainties due principally to calibration and background corrections range from 4% to 6.5% with increasing energy.

[b]Values derived by summing individual resonance capture and a small $1/v$ term.

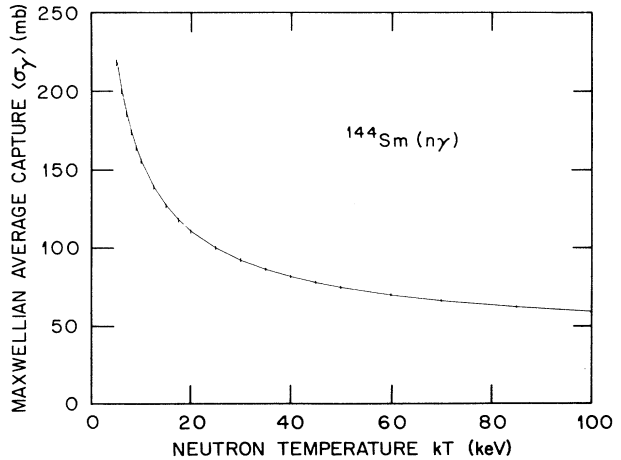

FIG. 4. Maxwellian average neutron capture $\langle\sigma v\rangle/v_T$ for ^{144}Sm for a range of temperatures appropriate to nucleosynthetic regions in stars. Numerical values are included in Table IV.

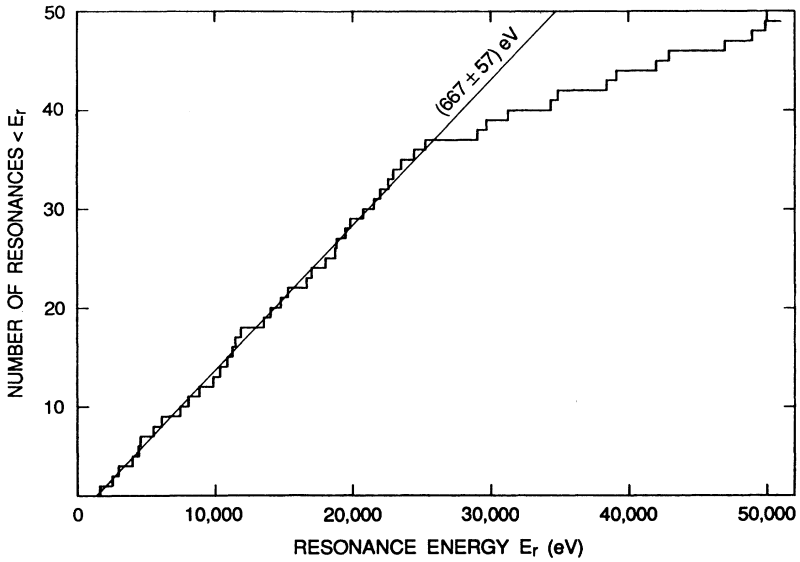

FIG. 5. The number of s-wave resonances found in ^{144}Sm up to neutron energy E_n as a function of energy. The slope of the solid line corresponds to a level spacing of 667 eV for the 37 resonances from 1 keV to 26 keV. The corresponding standard deviation for a Wigner spacing distribution is 57 eV.

wave strength function $S_0=(3.6\pm0.8)\times10^{-4}$. The distribution of the reduced neutron widths of the s-wave resonances below 26 keV is consistent with the Porter-Thomas distribution [17].

An s-wave radius R' of (5.38±0.03) fm was found from the interference effect of the fitted s-wave resonances, but it was inversely correlated (coefficient −0.54) with the noninterfering radius attributed to oxygen, moisture, and the few percent of isotopes other than ^{144}Sm in the sample. The noninterfering radius found was 10.8% above that calculated for oxygen in pure Sm_2O_3 and attributable to adsorbed moisture at 0.009 water molecule per molecule of samarium oxide.

IV. DISCUSSION

The average s-wave radiation width found, (74±5) meV, is in the range of values reported for neighboring mass numbers [18] but the few reported p-wave radiation widths near mass number 140 are near 40 meV, well below the 89 meV average we find for ^{144}Sm.

The 5- to 350-keV average capture cross sections of Kononov *et al.* [2] shown in Fig. 3 deviate both above and below the present results in various parts of the energy range. Their uncertainty decreases from ±20% at 10 keV to ±13% at 300 keV, whereas the uncertainty of the present results increases from about 4% near 10 keV to about 6.5% at 500 keV. The overall agreement of the two experiments seems quite good for such a small neutron-capture cross section.

The Maxwellian average cross section at 30 keV has been calculated with Hauser-Feshbach codes. Harris [19] found 165 mb and Holmes *et al.* [20] calculated 176 mb. Despite their close agreement we find a value of only 92±6 mb, a little more than half the calculated values. The uncertainty of the more global Holmes *et al.* calcula-

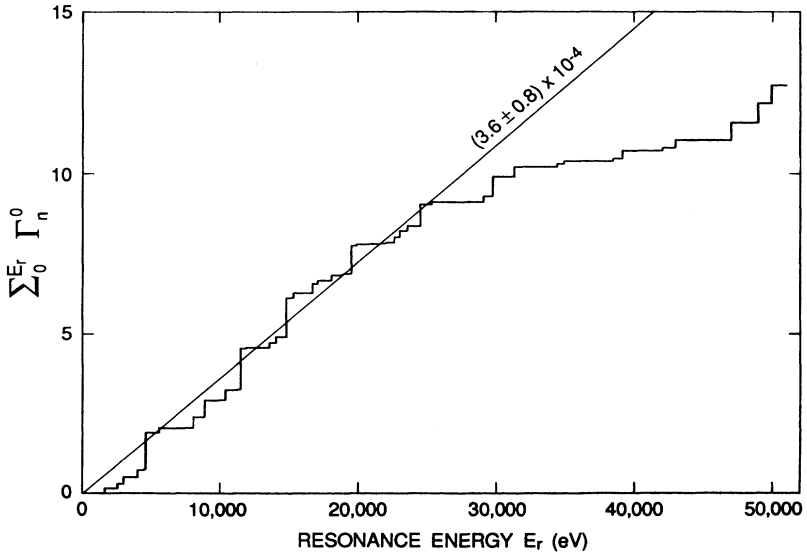

FIG. 6. The cumulative sum of s-wave reduced neutron widths as a function of energy. The solid line corresponds to a strength function $S_0=3.6\times10^{-4}$. The number of resonances (37) from 0 to 26 keV on which it is based imply a standard deviation of 0.8×10^{-4}.

tion is about a factor of 2, but the Harris calculations for other isotopes are often closer.

The capture resonance integral is an average, weighted with a $1/E_n$ spectrum starting at a lower limit of 0.5 eV, the cadmium cutoff energy. The experimental value from Alexander *et al.* [1] (2.38±0.17) b exceeds the (1.7±0.1) b computed from the resonances reported here. Because of the $1/E_n$ spectral weighting, this difference raises the question of possible missed ^{144}Sm resonances between 0.5 eV and 750 eV where the peaks seen have all been explained as due to the minor constituents in the sample (see Table I). The most likely energy of such a missed resonance would seem to be near 8 eV where the strong 8.047 eV ^{152}Sm+n resonance would easily obscure it. A $g\Gamma_n$ value of only 11×10^{-6} eV for an obscured ^{144}Sm resonance at that energy would contribute 0.68 b to the resonance integral and produce agreement with the measured resonance integral. The 0.65% ^{152}Sm content of our sample is calculated to give an effect equivalent to a resonance in ^{144}Sm at this energy of 200×10^{-6} eV.

The average level spacing for $J=1/2^+$ states of ^{145}Sm (determined from the spacing of s-wave resonances) of 670±60 eV is larger than expected considering those of the other $N=83$ nuclides at excitation energies just above their neutron separation energies. This is because the neutron separation energy for ^{145}Sm is 6.732 MeV and those for ^{143}Nd, ^{141}Ce, ^{139}Ba, and ^{137}Xe are only 6.123, 5.428, 4.723, and 4.026 meV, respectively. The corresponding average level spacings for the $J=1/2^+$ states for these four nuclides [18] just above the neutron binding energies are 440±50, 3200±200, 6300±1700, and $>10^5$ eV, respectively.

The s-wave neutron strength function for ^{144}Sm of $(3.8\pm0.8)\times10^{-4}$ is considerably larger than those of the other $N=82$ target nuclides. The values [18] for ^{142}Nd, ^{140}Ce, ^{138}Ba, and ^{136}Xe are $(1.5\pm0.4)\times10^{-4}$, $(1.1\pm0.3)\times10^{-4}$, $(1.6\pm0.4)\times10^{-4}$, and $\lesssim10^{-6}$, respectively. The s-wave strength function for other Sm isotopes from 147 to 152 range from 4.8 to 2.2×10^{-4}.

The 5.4-fm radius found for ^{144}Sm is distinctly smaller than the (8.3±0.2) fm reported [18] for ^{147}Sm, ^{149}Sm, and ^{152}Sm, but agrees well with a conventional deformed optical model calculation [18] for mass number 144. The s-wave strength function we find also agrees well with the same calculation at mass number 144 on the split 4S giant resonance peak.

V. CONCLUSIONS

Neutron capture and transmission measurements have been made from 0.5 eV to 500 keV and have been analyzed to give parameters of resonances up to ~100 keV. The average resonance spacing for s-wave resonances was determined to be 670±60 eV and the s-wave strength function $(3.6\pm0.8)\times10^{-4}$. The average radiation width for s-wave resonances was 74±5 meV and that for p-wave resonances somewhat larger ~89 meV. The Maxwellian average capture cross section at a stellar temperature of 30 keV was 92±6 mb. The capture resonance integral calculated from the resonance parameters and the thermal cross section of 1.7±0.1 b is somewhat smaller than the recently measured value of 2.38±0.17 b. This discrepancy might be explained if there were a small resonance in ^{144}Sm at ~8 eV which would have been obscured by the large resonance in ^{152}Sm at 8.047 eV, even though the ^{152}Sm is only present to 0.65% in the sample.

ACKNOWLEDGMENTS

We are particularly indebted to C. W. Alexander and J. Halperin of the Oak Ridge National Laboratory for suggesting the measurements and for fabricating and loaning us the samples. The ORELA operators and engineers provided the pulsed neutrons that made these measurements possible. This work was sponsored by the Office of Energy Research, Division of Nuclear Physics, U.S. Department of Energy, under Contract DE-AC05-84OR21400 with Martin Marietta Energy Systems, Inc.

[1] C. W. Alexander, J. Halperin, J. B. Knauer, and R. L. Walker, Nucl. Sci. Eng. **95**, 194 (1987).
[2] V. N. Kononov, B. D. Yurlov, E. D. Poletaev, and V. M. Timokhov, Yad. Fiz. **27**, 10 (1978) [Sov. J. Nucl. Phys. **27**, 5 (1978)].
[3] D. G. Gardner and M. A. Gardner, Lawrence Livermore National Laboratory Report UCID-20577, 1986.
[4] R. L. Macklin, D. M. Drake, and E. D. Arthur, Nucl. Sci. Eng. **84**, 98 (1983).
[5] H. Beer and R. L. Macklin, Astrophys. J. **339**, 962 (1989).
[6] R. L. Macklin, Nucl. Sci. Eng. **86**, 362 (1984).
[7] R. L. Macklin and J. H. Gibbons, Phys. Rev. **159**, 1007 (1967).
[8] R. L. Macklin, J. Halperin, and R. R. Winters, Nucl. Instrum. Methods **164**, 213 (1979).
[9] R. L. Macklin, N. W. Hill, and B. J. Allen, Nucl. Instrum. Methods. **96**, 509 (1971).
[10] N. W. Hill, J. A. Harvey, D. J. Horen, G. L. Morgan, and R. R. Winters, IEEE Trans. Nucl. Sci. **NS-32**, No. 1 (1985).
[11] C. M. Perey, J. A. Harvey, R. L. Macklin, F. G. Perey, and R. R. Winters, Phys. Rev. C **27**, 2256 (1983).
[12] R. L. Macklin, Nucl. Sci. Eng. **59**, 12 (1976).
[13] B. J. Allen, A. R. de L. Musgrove, R. L. Macklin, and R. R. Winters, in *Neutron Data of Structural Materials for Fast Reactors, Geel, 1977,* edited by K. H. Böckhoff (Pergamon, New York, 1979), p. 506.
[14] N. M. Larson and F. G. Perey, Oak Ridge National Laboratory Report ORNL/TM-7485, 1980; N. M. Larson, Oak Ridge National Laboratory Report ORNL/TM-9179/R2, 1989.
[15] E. P. Wigner, *Conference on Neutron Physics by Time of Flight,* Gatlinburg, 1956 (Oak Ridge National Laboratory Report ORNL-2309, 1957), p. 59.
[16] F. J. Dyson and M. L. Mehta, J. Math. Phys. **4**, 701 (1963).
[17] C. E. Porter and R. G. Thomas, Phys. Rev. **104**, 483 (1956).
[18] S. F. Mughabghab, *Neutron Cross Sections* (Academic, New York, 1984), Vol. 1, Part B.
[19] M. J. Harris, Astrophys. Space Sci. **77**, 357 (1981).
[20] J. A. Holmes, S. E. Woosley, W. A. Fowler, and B. A. Zimmerman, At. Data Nucl. Data Tables **18**, 305 (1976).